# Aerodynamic focusing of high-density aerosols

D.E. Ruiz [a,*], L.M. Gunderson [a], M.J. Hay [a], E. Merino [b], E.J. Valeo [b],
S.J. Zweben [b], N.J. Fisch [a,b]

[a] Princeton University, Department of Astrophysical Sciences, Princeton, NJ 08544, USA
[b] Princeton Plasma Physics Laboratory, Princeton, NJ 08543, USA

## ARTICLE INFO

## ABSTRACT

High-density micron-sized particle aerosols might form the basis for a number of applications in which a material target with a particular shape might be quickly ionized to form a cylindrical or sheet shaped plasma. A simple experimental device was built in order to study the properties of high-density aerosol focusing for 1 μm silica spheres. Preliminary results recover previous findings on aerodynamic focusing at low densities. At higher densities, it is demonstrated that the focusing properties change in a way which is consistent with a density dependent Stokes number.

© 2014 Elsevier Ltd. All rights reserved.

## 1. Introduction

Focusing effects in dilute aerosols have been the subject of many works (De La Mora & Riesco-Chueca, 1988; Liu et al. 1995a, 1995b; Wang & McMurry, 2006; Lee et al. 2013). In the dilute density regime, the aerosol particle movement can be modeled by a simple drag force within a prescribed background flowing gas. The particle-to-gas feedback effects are negligible since the aerosol density is small. This is usually the case in forensic applications, in which the density of the particulates is on the order of parts per million.

It was recently predicted that dense aerosols can be focused much like dilute aerosols (Hay et al., 2013). The dilute or low-density aerosol regime is defined as aerosols in which the particle mass density is much lower than that of the surrounding background gas upstream of the focusing. Correspondingly, in high-density aerosols, the particle mass density is comparable to or larger than that of the surrounding gas. Aerosol focusing in the high-density regime is more complex due to the strong coupling that arises between the aerosol particles and the surrounding background gas.

The focusing of an aerosol by an orifice is described by a dimensionless parameter, known as the Stokes number. It is defined as

$$St = \tau \frac{U_0}{D_0} = \frac{\rho_p D_p^2 C_s}{18 \mu_0} \frac{U_0}{D_0}, \tag{1}$$

where $\tau$ is the coupling time of the aerosol particles with the surrounding airflow, $U_0$ is the airflow velocity at the focusing orifice, and $D_0$ is the orifice diameter. The coupling time $\tau$ is a function of the particle density $\rho_p$, the particle diameter $D_p$, and the airflow dynamic viscosity $\mu_0$. A slip correction factor for the coupling time $\tau$ is given for low pressures in order to

---

* Correspondence to: Princeton Plasma Physics Laboratory, 100 Stellarator Rd., Plainsboro Township, NJ 08540, USA. Tel.: +1 609 243 3653.
  E-mail address: druiz@pppl.gov (D.E. Ruiz).

account for finite mean free path effects. It is defined as

$$C_s = 1 + Kn_p \left[ 0.77 + 0.40 \exp \left( -\frac{1.62}{Kn_p} \right) \right], \tag{2}$$

where $C_s$ is defined above for silica microspheres suspended in air (Fouks et al., 1964; Rader, 1990). $Kn_p$ is the Knudsen number, which is defined as the ratio of the background gas mean free path to the particle radius: $Kn_p = 2\lambda/D_p$. In this experiment, the gas mean free path was approximated by

$$\lambda = 60 \text{ nm} \frac{1 \text{atm}}{p}, \tag{3}$$

where $p$ is the local pressure near the orifice. For the present experiment, the slip factor coefficient $C_s$ varied from values of order unity to values near to $10^2$. Hence, including the slip factor correction is of vital importance when calculating the Stokes coefficient.

In previous studies, it was determined that a Stokes number of order unity, $St = \mathcal{O}(1)$, defines the condition for a focused aerosol beam (De La Mora & Riesco-Chueca, 1988; Liu et al., 1995a). When $St \ll 1$, the particles are strongly coupled to the gas flow, so particles follow the airflow lines closely and do not reach the axis of symmetry. Hence, no aerosol beam focusing occurs. On the other hand, when $St \ll 1$, the particles are weakly coupled to the gas flow, so the inward radial velocity of the particles can carry them through the axis. These conclusions have been experimentally validated for dilute aerosols, where the particle–particle interactions (such as coagulation) can be neglected (Liu et al., 1995b; Wang et al., 2006).

In the dense aerosol focusing regime, the particle focusing is modified by aberrations arising from the coupling of the particles with the background flowing gas. An intuitive example to illustrate high-density effects is the following: suppose that, in the dilute limit, the background gas parameters are set such that the aerosol is aerodynamically focused after passing the orifice. Keeping the gas mass flow fixed, when the particle density increases, the background gas will encounter more of the (slow moving) particles in the orifice. Hence, the speed of the background gas at the orifice decreases. By inspection of Eq. (1), we note that the Stokes number $St$ will also decrease at the orifice. By the results discussed in the previous paragraph, we can predict that at the high densities, the previously focused aerosol beam will become under-focused, i.e. the particle beam will have no focal point. Hence, finite aerosol densities can alter the focusing properties of the aerosol beam.

This leads to the notion of the effective Stokes number. The Stokes number shown in Eq. (1) is a function of the air flow velocity at the orifice. When no aerosol is present, one usually can infer the average velocity by measuring the air mass flow and the pressure nearby the orifice and applying simple mass conservation. However, when aerosol particles are present, calculating the perturbed background gas velocity field at the orifice is more difficult because the particle spheres may significantly perturb the surrounding gas flow. However, by the previous thought experiment for fixed mass airflow, we know that the velocity of the airflow should decrease when the aerosol density is significant. Therefore throughout this paper, the Stokes number calculations are made for the case of zero aerosol density, and we introduce the notion of the effective Stokes number which takes into account the reduction of the background gas velocity due to the aerosol density effect. By inspection of Eq. (1), the effective Stokes number tends to be smaller than the Stokes number when aerosol particles are present.

Recently, the self-consistent momentum coupling between the aerosol and the background gas flow was solved numerically (Hay et al., 2013). Hay et al. demonstrated through simulations that the optimal Stokes number needed for beam focusing shifts to higher values as the beam density increases. This can also be thought of as a decrease in an effective Stokes number for increasing aerosol densities.

In the present work, a simple experimental device was built to test the predictions of beam focusing in the high-density aerosol regime. Using 1 μm particles, we were able to experimentally observe the numerically predicted shift in the effective Stokes number. This work serves as a preliminary demonstration of the focusing of high-density aerosols which may be useful to produce beam targets for other experiments.

Focusing a dense aerosol may enable the formation of a dense slab of gas, which could be quickly ionized. The resulting dense slab of plasma, difficult to produce by any other means, may serve as a plasma coupler for laser amplification by stimulated Raman scattering (SRS) (Malkin et al., 1999; Toroker et al., 2012). Plasmas created by focused aerosols may be useful for SRS since the plasma medium will have a high electron density, be spatially homogeneous, and have a well-defined geometry. Another possible use of a high-aspect ratio dense plasma might be in Z-pinches (Slutz & Vesey, 2012, Sze et al., 2005).

This work is organized as follows: the experimental setup is described in Section 2. In Section 3, the experimental procedure is described. Section 4 presents the obtained results together with a discussion of them. Potential improvements to the experiment are also discussed in Section 4. Final concluding remarks are given in Section 5.

## 2. Experimental setup

A schematic view of this experiment is presented in Fig. 1. Air is stored in a sealed 100 L reservoir tank (A), initially at atmospheric pressure and temperature. This air continuously flows through this apparatus due to the pressure difference created by a roughing vacuum pump (P) [ALCATEL, MODEL 2033 of 23.3 m³/h displacement] at the other end of the system.

A convection vacuum gauge (B) [INSTRUTECH INC., SUPERBEE] is placed downstream the reservoir exit in order to measure the pressure variations inside the reservoir. A plug valve [NUPRO] is located downstream from the reservoir tank (C), and serves as the main air valve leading to the system. The air mass flow rate in L/min STP (Standard Temperature and Pressure) is measured with a thermal mass flow meter (D) [TSI INC., MODEL 4140]. The flow meter accuracy was $\pm 0.005$ L/min in our operating regime. The air mass flow rate is regulated by a needle valve (E) located downstream the flow meter, after which the pressure drops from close to atmospheric pressures to 0.5–60 Torr, as measured by a vacuum gauge (F) [INSTRUTECH INC., SUPERBEE]. The accuracy of the readings given by the pressure gauges was 100 mT in these conditions. The airflow is then divided into two flows using two plug valves (G,H) [NUPRO]: one flow goes directly into the mixing chamber, the other travels through a 6.35 mm diameter tube to the particle reservoir (I). This dual flow system allows some control over the aerosol density reaching the experimental chamber.

The aerosol is produced inside the particle reservoir (I), shown in Figs. 1 and 2. Before the apparatus is pumped down to vacuum, about 50 g of $SiO_2$ particle dust is inserted into a 2.54 cm diameter tube, which serves as the particle reservoir. As shown in Fig. 1, a variable fraction of the airflow can be directed through this reservoir. As the gas flows through the reservoir, particles are entrained by the air flow. In order to minimize the presence of large clumps of coagulated particles in the air stream from this reservoir, the reservoir is $\sim 50$ cm tall and positioned close to vertical, allowing the heavy coagulated particles to fall back into the reservoir by gravity. The aerosol density is varied by regulating the mass airflow coming into the particle reservoir and by occasionally striking the exterior wall of the reservoir to re-settle the powder column inside. This leads to a significantly variable aerosol generation density vs. time which propagates through the entire system on a timescale
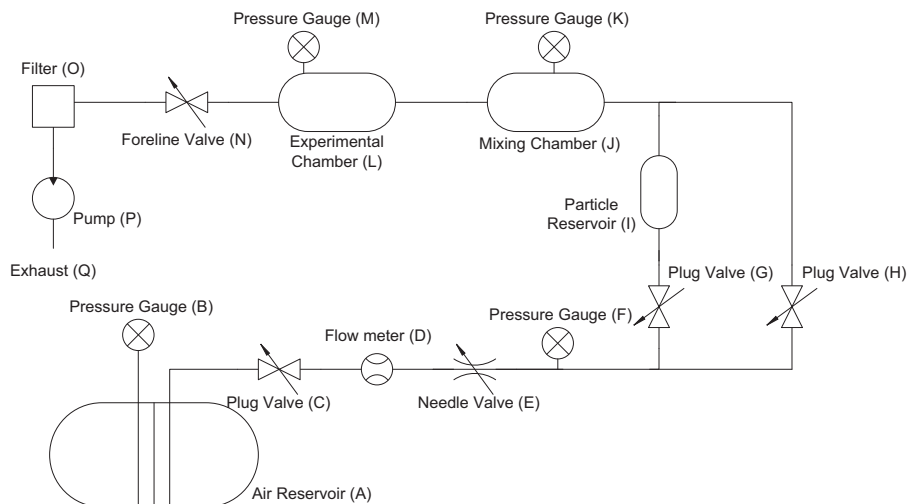


**Fig. 1.** Schematic of apparatus. The labels of each component will be referenced several times throughout the paper.
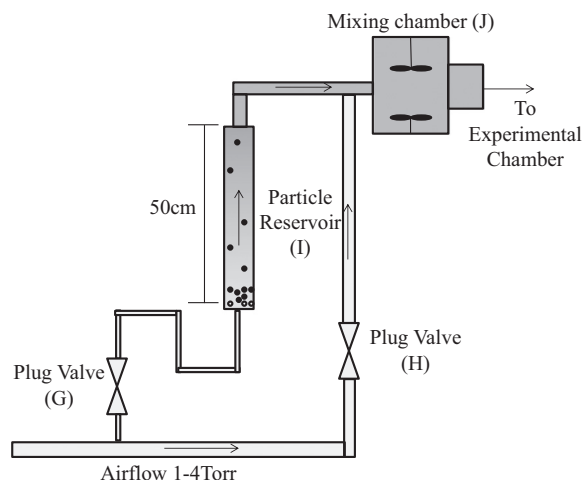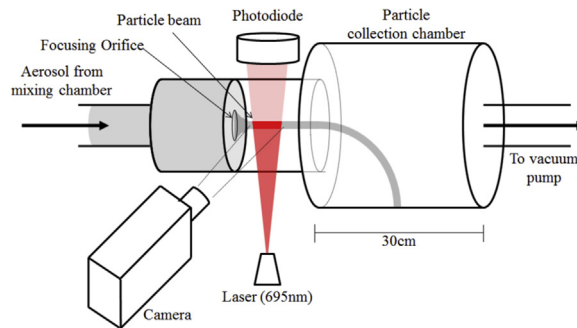


**Fig. 2.** Schematic view of apparatus during the aerosol production stage. The airflow is divided into two flows. One flow passes through the particle reservoir (I) and entrains particles with it. An aerosol (shown in dark color) is formed. The aerosol then travels into the mixing chamber, where electrical fans further homogenize the aerosol cloud. This diagram is not drawn to scale.

**Fig. 3.** Schematic view of apparatus during the focusing stage. The aerosol beam is diagnosed by a laser transmission measurement and a high definition camera. For optimized flow parameters, beam focusing can be achieved.

of $\sim 1$ s. These partially controlled variations in aerosol density generation are measured with high time resolution over experimental runs of $\sim 1$ h, and are used to map out the focusing properties vs. density discussed below.

Once the aerosol is produced, the aerosol flows into the mixing chamber (J), shown in Figs. 1 and 2. Inside the mixing chamber, small low voltage DC computer fans are installed in order to further mix the aerosol and make it more homogeneous. Another pressure gauge (K) [INSTRUTECH INC., SUPERBEE] is located nearby the mixing chamber. Since this pressure gauge was located in the vicinity of the mixing chamber, aerosol particles can flow into the pressure gauge and alter its functioning, causing at least an error of 30% on the pressure measurement.

After the mixing chamber, the aerosol flows into the experimental chamber (L) of Fig. 1 and passes through a 9 mm diameter focusing orifice, which is placed at the middle of a 10 cm diameter, 16 cm long pexiglass tube as shown in Fig. 3. Far downstream from the orifice and beyond the focal point of the particle stream, the aerosol flows into a larger 20 cm diameter, 30 cm long plexiglass tube. In this collection chamber, the airflow speed is further reduced, which allows the aerosol particles to fall by gravity and be collected. After passing through the experimental chamber (L), the airflow passes through the foreline valve (N) and is then evacuated through a stainless tube into a filter (O) to collect the remaining particles just before the vacuum pump (P).

Another pressure gauge (M) [INSTRUTECH INC., SUPERBEE] is located inside the particle collection chamber. The readings of this gauge and the mixing chamber gauge (K) are averaged in order to approximate the pressure at the focusing orifice and to calculate the Stokes number there. The pressure inside the chamber and the air mass flow rate are regulated by using the needle valve (E) and the foreline valve (N), located downstream from the collection chamber.

Regarding the aerosol beam diagnostics, the beam is characterized using optical techniques (Fig. 3). A 1 mW 695 nm red laser [STOKERYALE CANADA INC., LASIRIS] illuminates the focused aerosol beam from below. At the laser exit, a $30°$ single line projection head [EDMUND OPTICS] is added in order to create a light sheet 2 mm wide, which is aligned along the central axis of the focusing orifice. The scattered light by the aerosol beam is observed and recorded by a camera [PRINCETON INSTRUMENTS INC., PI-MAX 3] located orthogonal to both the laser sheet beam and the particle beam axis. The images are used to infer the beam diameter in the vertical direction. Above the particle beam, a photodiode [TERAHERTZ TECHNOLOGIES INC., PDA-750] is used to measure the laser light transmission through the aerosol beam. By using the beam diameter and the transmission measurement, the beam particle density is inferred by using Mie scattering theory (Mie, 1908).

A typical set of experimental conditions is summarized in Table 1. In this experiment, the aerosols were composed of silica 1 μm diameter particles [FIBER OPTIC CENTER INC.] with standard deviation $< 10\%$. The material density of the silica particles is approximately 1.8 g/cm$^3$. In Table 1, the shown air mass flow is approximately 0.1 L min$^{-1}$ STP (Standard Temperature and Pressure). During the experiments, the air mass flow was typically varied between 0.01 L/min and 0.500 L/min STP. Pressures inside the mixing chamber ranged from 0.6 to 40 Torr.

## 3. Methods

In this section, the experimental procedure is detailed. Before the experiment is pumped down to vacuum, the SiO$_2$ particles are inserted into the particle reservoir (I). After the vacuum pump is turned on and the pressure at gauge (M) reaches its limiting pressure of $\sim 600$ mTorr, the main plug valve (C), the needle valve (E) and the foreline valve (N) are opened in order to establish the desired air mass flow rate. In this phase, the plug valve (G) leading to the particle reservoir is closed. Having the air mass airflow constant, the chamber pressure is varied. For a fixed mass airflow, when the pressure inside the experiment chamber is changed, the background gas density, the airflow speed at the orifice and the slip correction factor $C_s$ are modified. These factors cause a change in the Stokes number. Different aerosol focusing regimes are accessed by following this methodology.

Once the desired mass flux and pressure conditions are set, the valve (G) controlling the airflow to the particle reservoir (I) is opened. The airflow then entrains particles from the reservoir and forms an aerosol. This effect only lasts for a few seconds, after which the easily entrained particles are spent, diminishing the aerosol generation. In order to solve this problem, the exterior of the particle reservoir is manually vibrated in order to produce more aerosol particles. To access

**Table 1**
Table showing typical measured parameters for a slightly over-focused aerosol beam in the dense regime.

| Quantity | Value |
| --- | --- |
| $SiO_2$ particle diameter | 1 μm $\pm$ 10% |
| Particle density | 1.8 g cm$^{-3}$ |
| Air mass flow | 0.100 L min$^{-1}$ STP $\pm$ 1% |
| Chamber pressure | 1.4 Torr $\pm$ 30% |
| Air density | 2.3 g m$^{-3}$ $\pm$ 30% |
| Air dynamic viscosity | $1.81 \times 10^{-5}$ kg m$^{-1}$ s$^{-1}$ |
| Gas velocity at orifice | 13 m s$^{-1}$ $\pm$ 30% |
| Slip factor $C_s$ | 77 $\pm$ 30% |
| Stokes number | 0.6 $\pm$ 30% |
| Beam width | 1.2 mm $\pm$ 10% |
| Normalized beam width | 0.13 $\pm$ 10% |
| Laser transmission fraction | 0.89 $\pm$ 0.1% |
| Mie Scatt. cross section | $3.1 \times 10^{-12}$ m$^2$ $\pm$ 10% |
| Aerosol particle density | $3 \times 10^{13}$ m$^{-3}$ $\pm$ 20% |
| Aerosol density | 29 g m$^{-3}$ $\pm$ 20% |
| Relative beam density | 12 $\pm$ 50% |
| Expected plasma density (fully ionized) | $8 \times 10^{18}$ cm$^{-3}$ $\pm$ 20% |

higher particle densities yet, the particle reservoir is tapped with a wrench causing more particles to be carried by the airflow stream. Although this rather crude method of producing the aerosol cannot directly control the aerosol mass density, it produces the wide variations of aerosol density needed to study the density effects on aerosol focusing.

Once the aerosol travels through the orifice inside the experimental chamber (L), the laser system illuminates the aerosol beam. The scattered light by the beam is recorded by the camera system. From the videos of the camera data, several properties of the focused beam are inferred, such as the beam diameter and the dispersion angle (aperture angle of the emerging aerosol beam). The light transmission measurement from the photodiode system located above the focusing orifice is used to infer the particle density inside the beam.

Regarding the data acquisition, all data measurements are recorded electronically by a LABVIEW program. The data acquisition frequency is held at 20 Hz. The raw data is later numerically treated and analyzed using a MATLAB algorithm.

Figure 4 shows an example of a typical transmission measurement. In this figure, at $t=7$ s the optical diode is blocked. This sharp decrease in the transmission measurement serves as a signal so that the data analysis can be easily done using a computer program. After the diode is unblocked, the particle reservoir (I) is vibrated in order to produce an outburst of aerosol. The resulting aerosol beam exiting the orifice decreases the light transmission. Once enough data is captured, the aerosol production is stopped and the diode is again blocked at the end in order to signal that the data acquisition has ended. Typical data acquisition time periods were about 20–40 s.

Once all the required data is acquired for the specific operating regime, the pressure inside the chamber is varied, causing a shift in the Stokes number and changing the focusing regime. After the system stabilizes (1–2 min) the data collection process is repeated. This process is repeated until a full parameter scan is made of the desired background gas variables. Typical experimental runs would last $\sim 1$ h before stopping in order to refill the particle reservoir with silica particles.

## 3.1. Analysis

The main parameters relevant to this experiment are the Stokes parameter, the aerosol beam diameter and the aerosol beam density. The first of these parameters describes the background aerosol flow conditions while the last two parameters characterize the resulting focused aerosol beam. In this subsection, we illustrate how to calculate such values from the available measurements.

The Stokes number in Eq. (1) is calculated by using the pressure and mass airflow measurements. By taking the mean of the pressure measurements given by gauges (K) and (M), one can approximate the pressure at the orifice. Then, we can obtain the air density at the orifice by using the expression: $\rho_{air} = 1.225(P/760 \text{ Torr})$ Kg m$^{-3}$. By combining the mass airflow measurement from (D), the calculated air density at the orifice and the orifice area, one can obtain the average velocity of the gas at the orifice by using mass conservation. Once the background gas velocity is calculated, the Stokes number can be easily obtained from Eqs. (1)–(3). An example of such calculations is given in Table 1.

To measure the particle beam width, a 2D profile image of the particle beam is obtained via the camera system (as an example for the reader, see Figs. 5). At approximately 20 mm downstream from the focusing orifice, a vertical profile cut of the scattered light intensity is obtained from the digitized images. This profile cut was later fitted to a Gaussian curve. The half-width of the fitted Gaussian is defined as the diameter of the aerosol beam.
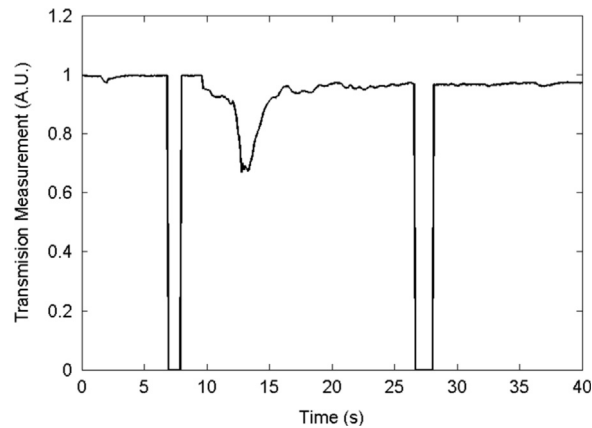
**Fig. 4.** Typical transmission measurement from the optical diode. The transmission measurement decreased by 25% in this example.
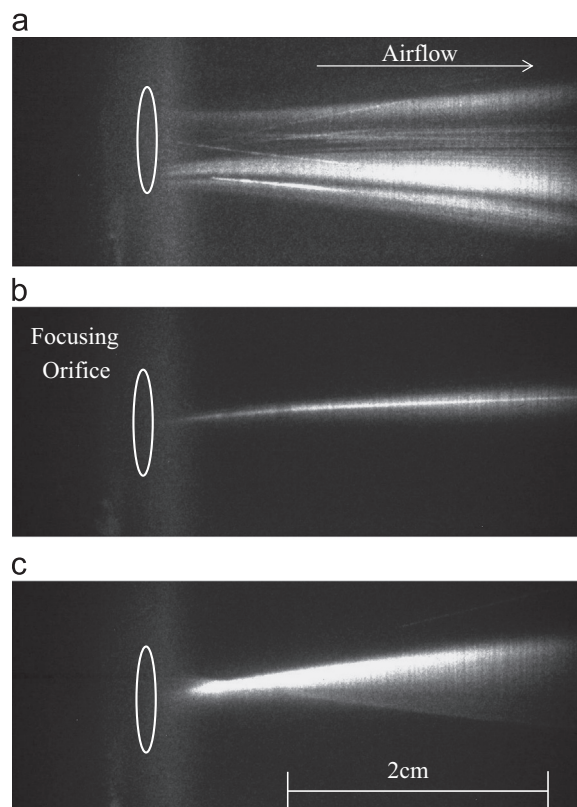


**Fig. 5.** Typical 2D profiles of the different aerosol focusing regimes. In these figures, the background gas flows from left to right. The focusing orifice is marked by the circles on the left hand side. (a) Example of under-focused regime. Particles still follow the flow streamlines. $St \simeq 0.2$. (b) Example of a good aerodynamic focusing regime. $St \simeq 0.6$. (c) Over-focused regime in which the aerodynamic focal point is clearly visible. $St \simeq 1.6$.

For the measurement of the beam density, the beam diameter is considered to be constant within the region where the laser light is directed towards the diode ($\sim 15$–25 mm from orifice). Hence, it is assumed that the beam diameter is constant along the line of sight of the diode. This is generally not true, but it gives a first approximation to the beam density. From the transmission measurement given by the photodiode, the $SiO_2$ particle density inside the beam is obtained by using the relation

$$T = \exp(-n_{beam}\sigma_p D_{beam}),  \tag{4}$$

where $T$ is the fraction of the transmitted light, $n_{beam}$ is the $SiO_2$ particle density (given in particles per unit volume), $\sigma_p$ is the Mie scattering cross-section of the particles and $D_{beam}$ is the measured diameter of the beam. In the case of 1 µm particles scattering 695 nm light (red), the Mie scattering cross section is approximately $\sigma_p \simeq 3.1 \times 10^{-12}$ m$^2$. Once $n_{beam}$ is
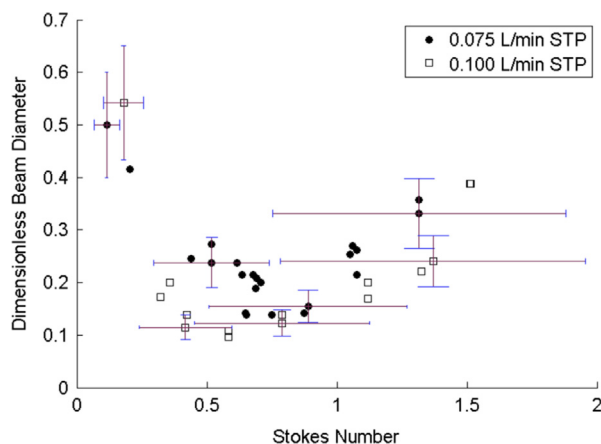
**Fig. 6.** Dimensionless beam diameter vs. Stokes number in the low aerosol density regime. For the shown airflow regimes, there exists an optimal Stokes number in which beam focusing is achieved.

determined, the mass density of the beam is calculated by using the expression

$$\rho_{beam} = n_{beam}\rho_{particle}V_{particle} \tag{5}$$

where $\rho_{beam}$ is the beam mass density, $\rho_{particle}$ is the particle mass density and $V_{particle}$ is the volume of each particle sphere. Data analysis for one case is presented in Table 1.

### 3.2. Uncertainties

We will discuss the main sources of uncertainty that are present for the calculation of the Stokes number, the aerosol beam diameter and the aerosol beam density.

For the calculation of the Stokes number, there are several sources of uncertainty, such as the calculation of the background gas velocity, the gas density at the orifice, and the distribution of the particle size. The first two are directly related to the measurement of the background pressure. The pressure measurement was subject to large errors because aerosol particles would consistently enter the vacuum gauges (K,M) and alter their functioning. Based on a comparison of the measurements given by gauges (K,M) at vacuum and at atmospheric conditions, before and after the experimental campaign, it is estimated that there is a 30% relative error in the pressure measurement. Uncertainties in the mass flow measurement are calculated to be on the order of 5%.

Another source of error in the calculation of the Stokes number comes from the uncertainty of the aerosol particle size. The particle manufacturer suggests a 10% uncertainty in the particle diameter. Further uncertainty arises since the method used to produce the aerosol surely creates particle agglomeration. Aerosol samples taken from the experiment showed evidence of such particle coagulation. If the rate of particle coagulation becomes important, the value of the calculated Stokes number would be underestimated (see Eq. (1)). We have not explicitly included this source of uncertainty in the estimated uncertainty of the Stokes number of around $\pm 50\%$.

In the measurement of the beam width, the uncertainty is mainly determined by the confidence intervals of the fitted Gaussian width of the scattered light profiles. It is estimated that the error of the beam width measurement is about 20%.

Regarding the uncertainty of the beam density, errors arise from the calculated Mie scattering cross-section, the beam width measurement, and the transmission measurement. For the calculation of the scattering cross-section, a 10% relative error is assigned since the cross-section directly depends on the uncertainty of the particle size. This error increases as particle coagulation becomes important. As previously stated, the error in the measurement of the beam width is 20%. Finally, two main sources of error in the transmission measurement exist. The first uncertainty is that the diode transmission measurement is an integrated measurement along the line of sight of the diode (1 cm along the axis). Along this distance, the aerosol beam diameter may vary. Hence, the obtained measurement can only give a coarse approximation of beam density. Second, there is the possibility that the beam emerging from the orifice is not always aligned to the orifice axis. Variations of the beam direction would cause an underestimation of the beam density. In summary, it is estimated that the uncertainty in the beam density measurement is of the order of 20%.

## 4. Results and discussion

### 4.1. Low-density regime

Typically observed beam focusing regimes are illustrated in Fig. 5. In the under-focused regime case (Fig. 5a), aerosol particles are tightly coupled to the carrier airflow and do not focus. The Stokes number for this image is $St \simeq 0.2$, lower than

the optimal Stokes number for focusing. From this image, it appears that the aerosol particles form streamlines that are aligned to the background gas flow.

An example of a good focusing regime is shown in Fig. 5b, where the Stokes number is approximately $St \simeq 0.6$. In this case, a clear focused aerosol beam is observed $\sim 0.5$–3 cm downstream from the orifice. As shown, the aerosol beam is also slightly deflected upwards. The exact reason for this deflection is not known. However, this is most-likely caused by the inhomogeneity of the aerosol upstream the focusing orifice; if so, this beam asymmetry is a flaw of the present aerosol generation technique.

Finally, the over-focused regime at $St \simeq 1.6$ is presented in Fig. 5c. After the orifice, the particles continue in straight paths due to low coupling with the gas. When the particles cross the orifice axis, an aerodynamic focal point can be observed.

These three examples illustrate the typical focusing regimes that were observed during the experimental runs in the dilute aerosol regime. For Fig. 5, no beam density measurement was available, but these images were probably in the dilute, low density aerosol regime.

In this low density regime, the ratio of the particle mass density inside the beam $\rho_{\text{beam}}$ and the background gas $\rho_{\text{gas}}$ is $\rho_{beam}/\rho_{gas} < 1$. In Fig. 6, the dimensionless particle beam diameter is plotted versus the Stokes number. The dimensionless beam diameter is defined as the diameter of the beam measured at $\sim 20$ cm downstream from the orifice divided by the orifice diameter. Two data sets are included corresponding to mass air flows of 0.100 L/min STP and 0.075 L/min STP. As it can be seen for both data sets, there exists an optimal Stokes number that focuses the aerosol beam. For the case of the 0.100 L/min air flow, the minimum is located at a Stokes number of $St \simeq 0.6$, and in the case of the 0.075 L/min airflow, the optimal Stokes number was $St \simeq 0.75$. The observed focused beam diameter was $7 \times -10 \times$ smaller than the focusing orifice of 9 mm diameter.

## 4.2. High-density regime

In this section, the behavior of the aerosol focusing properties in the dense regime is studied. As mentioned in Section 1, it is predicted that when the particle density in the aerosol increases, the velocity of the background is reduced. Thus, there is a change in the focusing regime. Figures 7 and 8 compare aerosol beams with different particle aerosol density in the same background gas flow conditions. On the left hand side, the 2D scattered light profiles are shown. On the right hand side, a profile cut of the scattered light is shown. In Fig. 7, the airflow characteristics are set in order to have a slightly
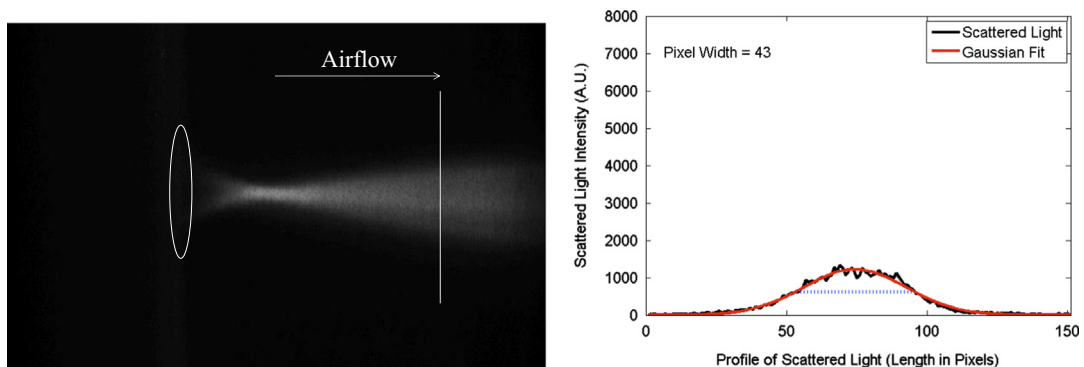


**Fig. 7.** 2D profile and intensity profile of the scattered light from the particle beam at low aerosol densities with $\rho_{beam} < \rho_{gas}$. The scattered light profile is taken from a vertical cut 2 cm away from the orifice.
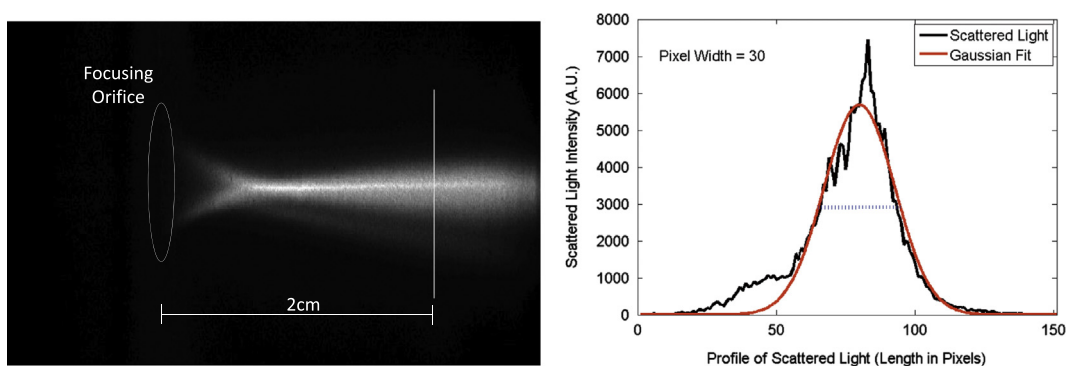


**Fig. 8.** 2D profile and intensity profile of the scattered light from the particle beam at high aerosol densities $\rho_{beam} > \rho_{gas}$.

over-focused beam ($St \simeq 0.66$) in the low-density regime. In Fig. 8, the aerosol particle density is increased while having the flow Stokes number constant. Comparing the respective scattered light profiles, the high-density particle beam appears to be better focused, at least qualitatively consistent with the theory made that the effective Stokes number decreases (Hay et al., 2013).
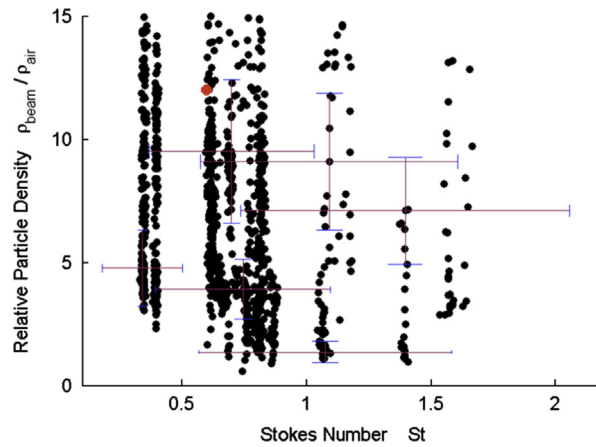


**Fig. 9.** Each data point represents a measurement of the beam width at a certain beam density and flow Stokes number regime. The data shown in Table 1 and Fig. 12 is represented by the data point shown in red. (For interpretation of the references to color in this figure caption, the reader is referred to the web version of this paper.)
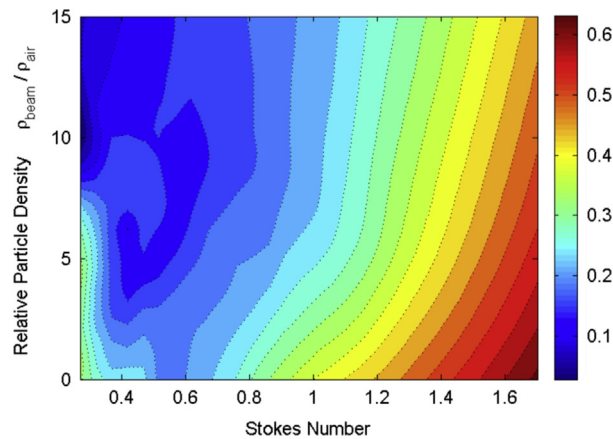


**Fig. 10.** Contour plot of the normalized beam width (beam width/orifice size) vs. the Stokes number and the normalized aerosol density.
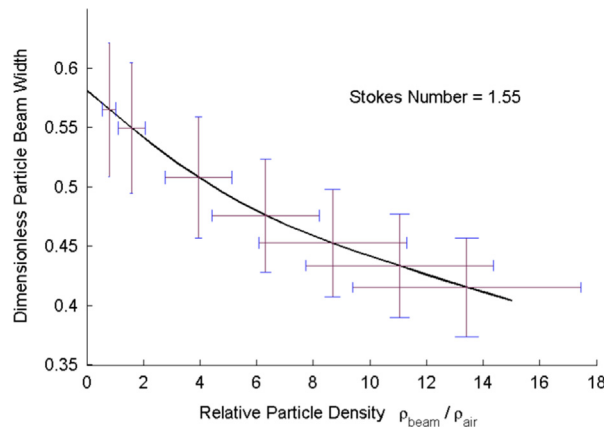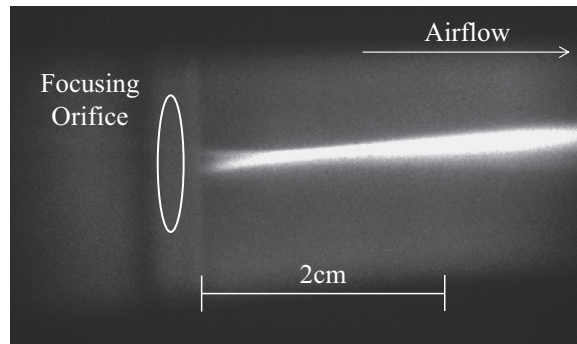


**Fig. 11.** In the over focusing regime, as the beam density increases, the background gas tends to slow down. This causes the effective Stokes number to decrease. Hence, the beam tends to focus better.

**Fig. 12.** Example of aerosol beam slightly over-focused in the dense regime. The characterization data of this beam is given in Table 1.

Figure 9 presents the entire set of experimental points of the aerosol beam density vs. the Stokes number. A 3-D surface of the normalized beam width $D_{beam} = D_{beam}(St, \rho_{beam})$ as a function of Stokes number and beam density was obtained by making a linear regression of all these three measurements for the experiment data points in Fig. 9. The contour plot of the constructed surface is shown in Fig. 10. As it can be seen, the optimal Stokes for focusing in the dilute regime is $St \simeq 0.55$ (this agrees with the minimum shown in Fig. 6). For larger Stokes numbers, it appears that when the beam density increases at a given Stokes parameter, the beam width decreases. Hence, a beam that is initially over-focused in the dilute regime can become better focused in the dense regime, as illustrated in Figs. 7 and 8.

As shown in Fig. 10, the particle density effects on aerosol beam focusing seem to be more apparent for regimes in which the Stokes number is high. From the interpolated surface in Fig. 10, a cut at a constant Stokes number, $St \simeq 1.55$, is shown in Fig. 11. This figure illustrates the dependence of an over-focused beam width on the beam density. This effect might be useful for the design of aerosol beams that could serve as targets for plasma related experiments.

A set of typical operating parameters was summarized in Table 1. The numbers shown represent a slightly over-focused aerosol beam in the dense regime, as in Fig. 12. The data point of this beam is shown in red in Fig. 9. As shown, the aerosol mass density is $10\times$ larger than the background gas mass density inside the particle beam. If such beam were to be completely ionized, the resulting plasma density would be of $8 \times 10^{18}$ cm$^{-3}$. This regime could be of interest for SRS or Z-pinch applications mentioned in Section 1.

### 4.3. Potential Improvements

The apparatus used for this experiment was simple, and many improvements can be contemplated. First, the method for the aerosol generation could be improved. The current methodology produced high-density aerosols that varied significantly in time (as it can be seen in the light transmission measurement in Fig. 4) and were not always axially symmetric, as can be seen in Figs. 5, 7, 8 and 12. Moreover, the velocity distribution of the aerosol particles upstream from the orifice was not known. These factors caused the aerosol beams to often show irregular, unpredictable behavior, such as strong anisotropies, density fluctuations, and vertical deflection. Also, particle agglomeration very likely occurs for the particular method of aerosol generation deployed here. These effects cause additional difficulties on the characterization of the aerosol beam. For future work, better methods of aerosol production and measurement should be devised in order to improve the accuracy of these experiments, e.g. direct measurements of the degree of agglomeration within the airflow itself.

Regarding future improvements on the diagnostics, the pressure gauges in direct contact with the aerosol gas could be better protected in a way to prevent particles from getting into the gauges. Also, camera imaging from two perpendicular directions would be useful to measure beam deflection on both directions. Finally, the silica particle velocity distribution could be measured via PIV or ultrasonic methods.

The typical chamber pressures measured in the experimental chamber (J) during focusing were close to 1 Torr. For use in plasma experiments, it would be more convenient if aerodynamic focusing occurred was achieved at lower chamber pressures. This could be accomplished by using smaller aerosol particles, larger focusing orifices, and/or smaller air mass flow rates. As an example, it is predicted that for 10 nm silica particles traveling through a 5 cm focusing orifice in a 0.01 L/min background gas airflow, optimal focusing would occur at pressures near 1 mTorr. Alternatively, the background gas can also be expanded by using a supersonic nozzle located downstream from the focusing orifice. These improvements would produce a more isolated particle beam. If such particle beams were to be ionized, the resulting plasma column could be better characterized by using standard plasma diagnostics.

## 5. Conclusions

This work was a preliminary experimental effort to study the effects of aerosol density on aerosol aerodynamic focusing. Our main result was to demonstrate the particle density dependence of aerosol focusing. The control over particle density in

this experiment was crude, so that the aerosol density had to be inferred rather than simply programmed. Also, the method of aerosol production was subject to particle coagulation, which introduced uncertainties in the effective particle size. However, by analyzing different density cases, the general trend of focusing with an effective-media Stokes number was observed, consistent with the numerical predictions reported earlier (Hay et al., 2013). The main consequence of this so-called "density effect" is that slightly over-focused aerosol beams in low density regimes become better focused when the aerosol density is increased.

## Acknowledgments

## References

De La Mora, J.F., & Riesco-Chueca, P. (1988). Aerodynamic focusing of particles in a carrier gas. *Journal of Fluid Mechanics, 195,* 1–21.

Fouks, N., Daisley, R., Davies, C., & Fouks, M. (1964). *The Mechanics of Aerosols.* New York: Paris.

Hay, M.J., Valeo, E.J., & Fisch, N.J. (2013). Geometrical optics of dense aerosols: Forming dense plasma slabs. *Physical Review Letters, 111,* 188301.

Lee, K.-S., Hwang, T.-H., Kim, S.-H., Kim, S.H., & Lee, D. (2013). Numerical simulations on aerodynamic focusing of particles in a wide size range of 30 nm–10 μm. *Aerosol Science and Technology, 47,* 1001–1008.

Liu, P., Ziemann, P.J., Kittelson, D.B., & McMurry, P.H. (1995a). Generating particle beams of controlled dimensions and divergence: II. theory of particle motion in aerodynamic lenses and nozzle expansions. *Aerosol Science and Technology, 22,* 293–313.

Liu, P., Ziemann, P.J., Kittelson, D.B., & McMurry, P.H. (1995b). Generating particle beams of controlled dimensions and divergence: II. experimental evaluation of particle motion in aerodynamic lenses and nozzle expansions. *Aerosol Science and Technology, 22,* 314–324.

Malkin, V.M., Shvets, G., & Fisch, N.J. (1999). Fast compression of laser beams to highly overcritical powers. *Physical Review Letters, 82,* 4448–4451.

Mie, G. (1908). *Annalen der Physik, 25,* 377–445.

Rader, D.J. (1990). Momentum slip correction factor for small particles in nine common gases. *Journal of Aerosol Science, 21,* 161–168.

Slutz, S.A., & Vesey, R.A. (2012). High-gain magnetized inertial fusion. *Physical Review Letters, 108,* 025003.

Sze, H., Banister, J., Failor, B.H., Levine, J.S., Qi, N., & Velikovich, A.L., et al. (2005). Efficient radiation production in long implosions of structured gas-puff pinch loads from large initial radius. *Physical Review Letters, 95,* 105001.

Toroker, Z., Malkin, V.M., Balakin, A.A., Fraiman, G.M., & Fisch, N.J. (2012). Geometrical constraints on plasma couplers for Raman compression. *Physics of Plasmas, 19,* 083110.

Wang, X., Kruis, F.E., & McMurry, P.H. (2006). An experimental study of nanoparticle focusing with aerodynamic lenses. *International Journal of Mass Spectrometry, 258,* 30–36 (Aerosols/Microparticles Special Issue).

Wang, X., & McMurry, P.H. (2006). A design tool for aerodynamic lens systems. *Aerosol Science and Technology, 40,* 320–334.